

# Enhanced Photocatalytic Activity with sulphur rich CuS Nanoparticles Grown by Hydrothermal Route

UPS. Gahlaut, Y. C., Goswami<sup>\*</sup> and Jyoti Bala  
Nano Research Lab, Department of Physics, SOS,  
ITM University Gwalior, MP 474001, India

## Abstract.

Highly active CuS nanoparticles (NPs) were synthesized using a hydrothermal route with various sulphur ratios. The comprehensive characterization of these NPs involved an analysis of their structure, composition, and optical properties, primarily conducted through X-ray diffraction (XRD) analysis. The XRD pattern confirmed the presence of the hexagonal phase in the CuS particles. The investigation further determined an estimated bandgap energy of 3.80eV for the slightly sulphur-rich CuS NPs. Notably, this energy value exceeds that of bulk CuS, indicating a noticeable miniaturization effect. The novel CuS NPs exhibited outstanding photocatalytic activity in the degradation of methyl Red (MR), particularly under visible light. This impressive performance is attributed to surface-bound OH ions on the CuS nanostructures, facilitating the adsorption and acceleration of the degradation process for MR molecules under visible light irradiation. The research highlights the significant promise and efficiency of the synthesized CuS NPs as photocatalysts. These nanoparticles are particularly responsive to stable visible light, making them highly suitable for purifying chemically contaminated wastewater. Specifically, their effectiveness in degrading stable azo dyes, exemplified by MR, underscores their potential in practical applications.

**Keywords:** Photocatalysts; CuS; Hexagonal; Optical properties; Hydrothermal; Nanostructures

## 1. Introduction

Semiconductor nanomaterials exhibit distinct properties compared to their bulk counterparts, driven by factors such as their surface-to-volume ratio and confinement of electrons within three dimensions [1-4]. These unique attributes have sparked considerable interest in their exploration. Transition metal chalcogenides, due to their novel physical and chemical characteristics, have recently garnered substantial attention. Metal sulphides, as a significant class of semiconductors, offer tuneable band gaps via control over particle size. Among these sulfides, CuS stands out as an exceptional semiconducting material with vast potential across domains. Copper sulphide is a p-type semiconductor that possesses a crystalline phase-dependent band gap spanning 1.48eV to 2.89eV [5]. This range notably aligns with the energy spectrum of ultraviolet and visible light [6]. like solar cells, photocatalysis, supercapacitors,

photothermal conversion, and surface plasmon resonance absorption. This intriguing alignment underscores CuS strong capacity for absorbing ultraviolet and visible light suitable for applications like photocatalytic pollutant degradation [7]. Placement of HOMO (Highest occupied Molecular Orbit) and LUMO (Least Occupied Molecular orbit) of CuS on energy scale at 5.1 eV and 2.9 eV respectively enable CuS nanostructures applications in **solar cell** [8-9]. High energy Capacity ( $560 \text{ mA h}^{-1} \text{ g}^{-1}$ ) and good electronic conductivity ( $10^3 \text{ S}^{-1} \text{ cm}^{-1}$ ) enables CuS application as a good material for cathode in **lithium batteries** [9-10]. A recent research article has also reported use of CuS as glucose and DNA **sensor** [11]. Due to their better physiochemical and pharmacokinetics characteristics than gold, silver nanomaterial copper sulphide nanostructures have attracted attention in **biomedical field**. [11] CuS nanostructures can absorb from 400 to 550 nm because of their unique size dependent properties and provide a strong blue emission band at 465 nm. This makes CuS an excellent photo luminescent material which enables its use in biological labelling, and in **light emitting devices**. [9] Recent research papers show that CuS nanorods can transmit 50% of visible light (300-650 nm). This transparency in the UV and near IR region enables use of CuS in spectrally **selective window coatings**. [12]. The physicochemical attributes of CuS undergo significant alterations upon scaling down to the nanoscale, owing to the quantum size effect. Wang (2016) [13] reported the application of CuS nanoparticles in imaging and cancer therapy. Similar work also reported by Gold/hydroxypropyl cellulose hybrid nanocomposites and Bi-Oxide nanoparticle ZnO/CuO [14-15]. He et al. (2012) studied peroxidase-like activities with the help of CuS and their superstructures [16].

Various synthesis methods have been reported to synthesise CuS nanostructures [17], including solvothermal (Cheng et al. 2010), (2013), thermolysis, sonochemical, and hydrothermal approaches [18-21]. Among these, the hydrothermal method has emerged as a prominent technique, primarily due to its versatility and reproducibility. The morphologies of CuS nanoparticles are strongly influenced by precursor concentration, surfactant presence, and reaction parameters like temperature and duration [22-26]. Many Research groups have reported Photocatalytic activity of CuS nanoparticles on dyes like MB (Methylene blue), CR (Congo Red), RhB (Rhodamine B), [27-29] with percentage degradation ranging from 50 to 94. In comparison to them not only our percentage degradation 96 is higher but our preparation method is fast, simple, ecological and low-cost.

In the present work, we successfully synthesized intriguing copper sulphide nanostructures employing a simple and cost-effective hydrothermal method, where ethylene glycol (EG) served as the surfactant, and water functioned as the solvent. The surfactant played a pivotal role in determining CuS morphology and conferring stability to the nanostructures [30]. The synthesis process employed copper chloride and thiourea as copper and sulphur sources, respectively, in the presence of EG surfactant at  $150^\circ\text{C}$  for four hours, with varying concentrations of thiourea. CuS, a p-type semiconductor is known for its excellent photocatalytic degradation activity and superior absorption of solar radiation, making it an ideal candidate for dye removal applications [31-32]

## **2. Experimental Details**

### **2.1 Materials Used**

Thiourea, Copper chloride, and Ethylene glycol (EG) were utilized as received, without the need for further purification. These chemicals were of analytical reagent (AR) grade and were procured from Sigma Aldrich. Distilled water, freshly prepared, was employed as the solvent during the synthesis.

### **2.2 Synthesis Steps**

The synthesis comprised three distinct steps:

#### **2.2.1 Preparation of Solvent**

A solvent was first prepared by blending 30mL of distilled water with 70mL of ethylene glycol (EG), with continuous stirring for 30minutes. Following vigorous stirring, the resulting solution was divided into four equal portions.

#### **2.2.2 Preparation of Copper Sulfide Solution**

In the initial portion of the solvent, a mixture of 0.1M CuCl and 0.1 M thiourea was dissolved within a beaker, which was subsequently subjected to ultrasonication for an hour at 40°C. Subsequently, CuCl and thiourea were mixed in varying ratios of 1:1, 1:3, 1:5, and 1:7. These mixtures were then placed in an autoclave and maintained at 150°C for a duration of 4 hours. This process was replicated for each of the three ratios. After aging for three days, the resulting solutions were labelled S1, S2, S3, and S4, corresponding to the different ratios.

#### **2.2.3 Photocatalytic Experiment**

Photocatalytic experiments were conducted employing ammonia-doped CuS nanostructures to catalyze the decomposition of a dye. A 10ppm solution of methyl red was prepared, maintaining a pH of 6. The absorbance maximum of methyl red was identified at 464 nm, serving as the reference wavelength for all absorbance measurements. In each of the four separate beakers, 20mL of the methyl red solution was dispensed, followed by the addition of 0.2g of photocatalyst powder. Subsequent stirring ensued within a dark environment before transferring the beakers to a self-constructed photocatalytic reactor outfitted with a 36-watt white light source. The reaction rate was assessed utilizing Beer-Lambert's law (Eq. (1)), and the rate constant (k) was determined employing Eq. (2).

$$\text{Degradation \%} = \left(1 - \frac{A}{A_0}\right) \times 100 \dots\dots (1)$$

Where A is concentration of dye at time t and A<sub>0</sub> is concentration of initial time t=0. for rate constant we used another equation

$$K = \log (A_0/A)/t \dots\dots\dots (2)$$

## 2.3 Characterization

X-Ray Diffraction (XRD) Analysis were carried out using a 300/650 Miniflex instrument. The analysis spanned a 2θ range from 20° to 80°. Fourier Transform Infrared (FTIR) Analysis Functional analysis was conducted using a Perkin Elmer instrument. UV-Visible Absorption Studies Absorption studies were performed using a Perkin Lambda – 25 UV-Visible Spectroscopy instrument. Photoluminescence (PL) Studies Photoluminescence (PL) studies were carried out using a Perkin Elmer LS-55 instrument at PC Ray Centre, ITM University, Gwalior.

## 3. Results and discussions

### 3.1 Structural Characterization

The XRD spectra of the synthesized CuS nanostructures at different precursor ratios (a) 1:1 (b) 1:3 (c) 1:5 and (d) precursor ratio 1:7 shown in Fig.1. Spectra indicate that all apparent peaks are assigned to the hexagonal crystal structure of CuS (JCPDS 78-0876), with no additional peaks. The XRD results indicate the high purity of the hydrothermally synthesized products. This result is in good agreement with previous reports showing multiphase CuS. All [33] diffraction peaks of the CuS crystal structure are identified.

The crystallite size (D) and microstrain (ε) of the resulting CuS nanocomposites can be calculated from the XRD patterns using Williamson Hall analysis [34] (graph in Fig. 2). The first is responsible for the crystallite size (D), and the second reflects the strain effect (ε):

$$\beta = \beta_D + \beta_\epsilon \dots\dots\dots (3)$$

The Williamson-Hall equation can be written as in the following:

$$\beta \cos\theta = k \frac{\lambda}{D} + 4\epsilon \sin\theta \dots\dots\dots (4)$$

The crystallite size of CuS nanocomposites is calculated using Debye Scherer equation [35]. The calculated microstrain of material is 0.77 nm for all samples and has the same fringe width. The particles exhibit the same size 75.10 nm approximately. And have a negative slope. All the samples exhibit almost identical data there is no change in XRD data. The slope is negative confirming the presence of compressive strain.

$$D = 0.9\lambda / \beta \cos\theta$$

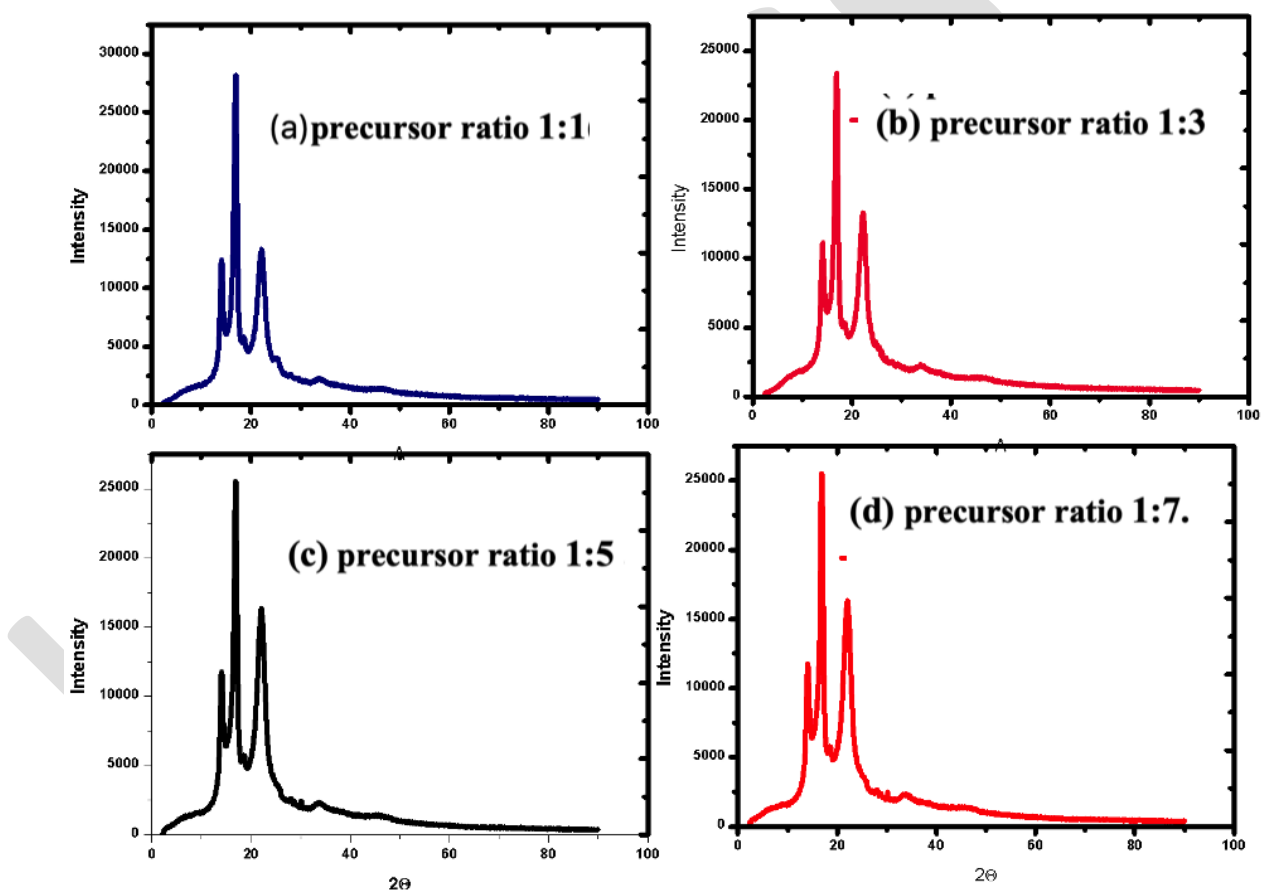


**Fig. 1** X-Ray diffractograms of CuS nanocomposite (a) precursor ratio 1:1 (b) precursor ratio 1:3 (c) precursor ratio 1:5 and (d) precursor ratio 1:7.

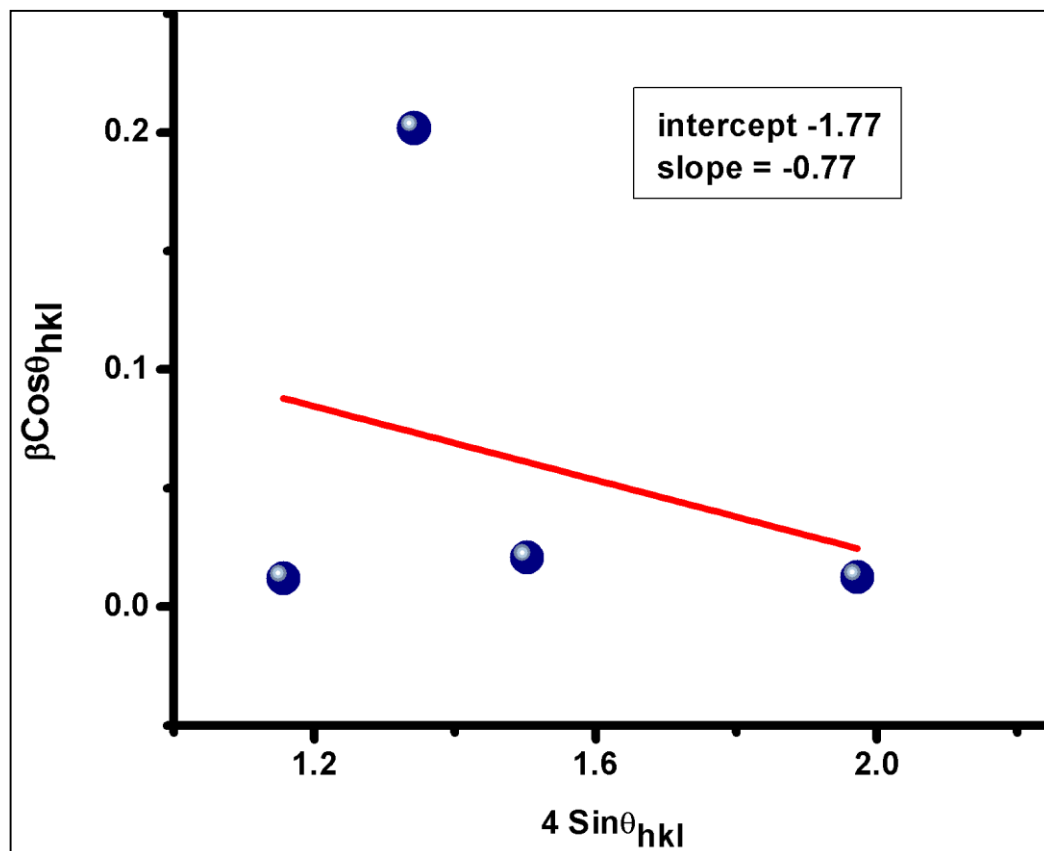


Fig. 2 W-H Plots of CuS nanocomposite.

### 3.2 FTIR Studies

Fig. 3. IR spectroscopy shows that CuS and its complexes have properly prepared a peak residing at  $3358 \text{ cm}^{-1}$ . This corresponds to the stretching frequencies of epoxide C-O bonds and dangling -OH bonds [36]. The intensity of the peak increases with the addition of S nanoparticles to CuS. The peak at  $1588 \text{ cm}^{-1}$  is assigned to the extension frequency of carbonyl C=O bonds and the peak at  $1386 \text{ cm}^{-1}$  indicates  $\text{CH}_2$ . The peak at  $631 \text{ cm}^{-1}$  indicates a stretching vibration. Table 1 shows all the peaks obtained from the IR data [37].

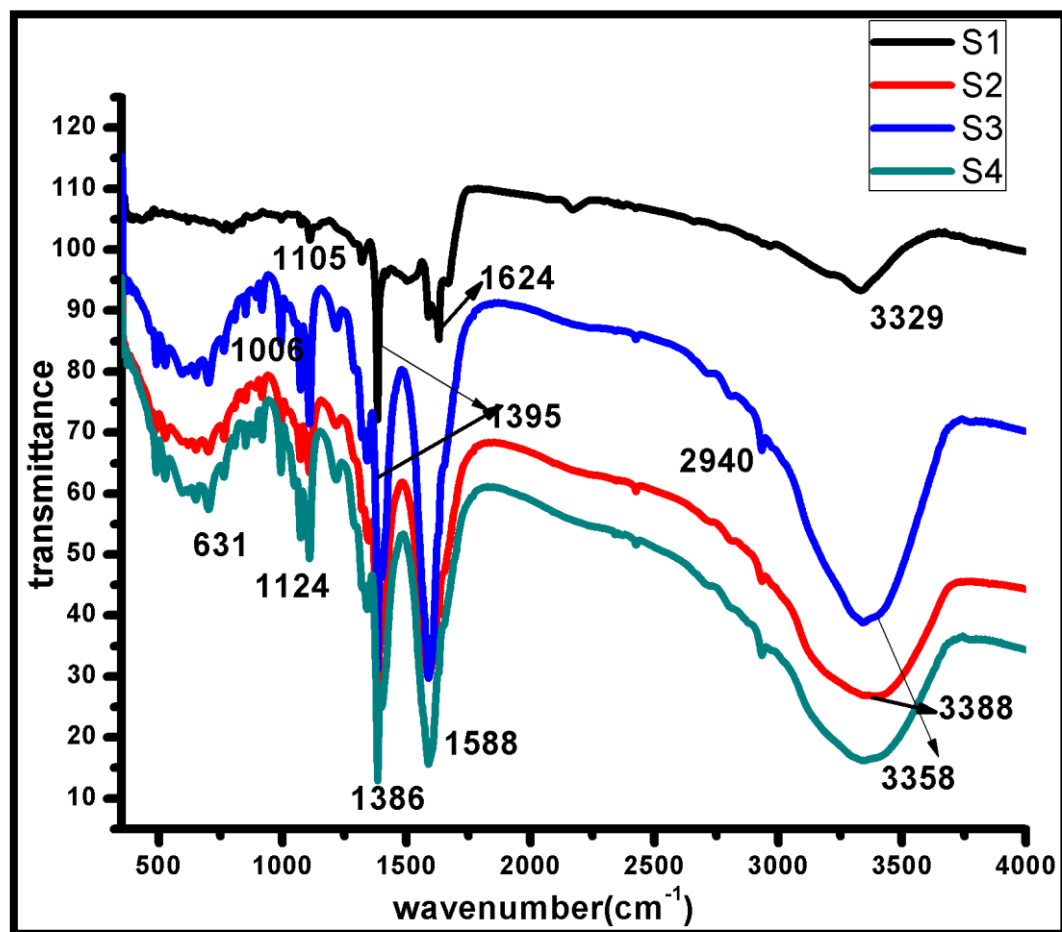


Fig. 3 FTIR-Spectrum Bands Wave numbers  $\text{cm}^{-1}$  attributed stretching vibrations.

**Table1** IR-Spectrum Bands Wave numbers  $\text{cm}^{-1}$  attributed stretching vibrations

Stretching	S1	S2	S3	S4
	Wavenumber $\text{cm}^{-1}$			
O-H stretching	3358	3388	3358	3329
C=C	1588	1588	1588	1624
C-C	1386	1395	1395	1395
C-H	1124	1124	1006	1105
Cu-S	631	631	631	631

### 3.3 Optical Studies

The optical bandgap ( $E_g$ ) of CuS at various proportions of S in CuS (a) precursor ratio 1:1(b) precursor ratio 1:3 (c) precursor ratio 1:5 and (d) precursor ratio 1:7 was calculated with the help of Tauc relation and absorption spectra [38-40] shown in Fig. 4.

$$(\alpha h\nu)^2 = A((h\nu - E_g))$$

Where  $h\nu$  is the photon energy  $\alpha$  absorption coefficient.  $E_g$  is the optical bandgap. The values of the optical bandgap  $E_g$  of the CuS nanocomposite sample were determined to be (a) 3.80eV (b) 3.85eV (c) 3.83eV (d) 3.7eV. The optical bandgap of CuS nanocomposites decreases with increasing concentration of Sulphur in CuS. The decrease in the bandgap of CuS can be explained by the increased surface charge between Cu and S, resulting in a shift of the optical bandgap to longer wavelengths. The S2 and S3 samples have slightly larger band gaps than the S1 and S4 samples

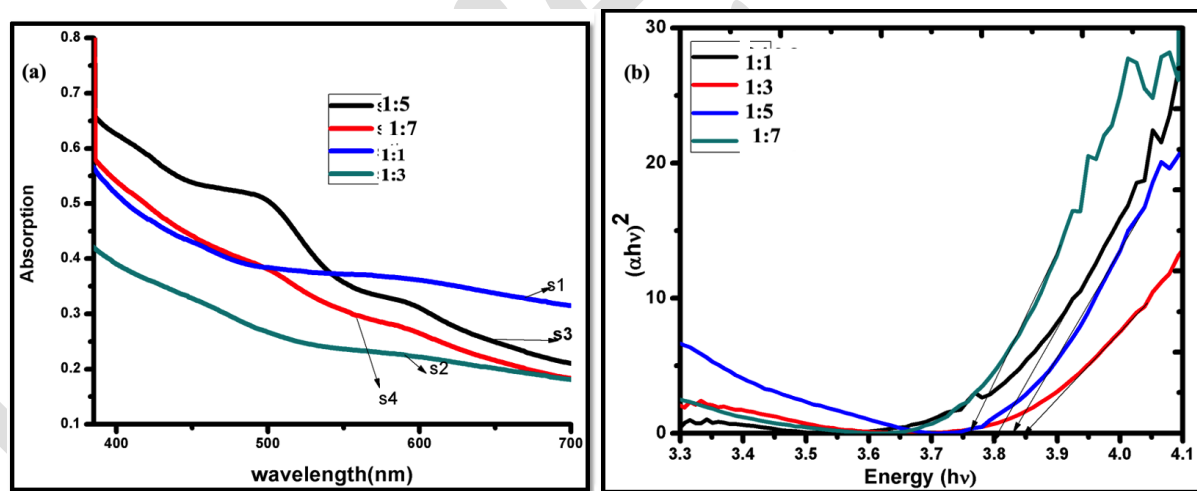


Fig. 4 (a) Absorption spectra and (b) tauc plot of CuS nanostructures grown with various precursor ratios 1:1, 1:3, 1:5 and 1:7.

### 3.4 Photoluminescence studies (PL)



Photoluminescence spectra for CuS samples were carried out shown in Fig. 5. Broad Peak at 350nm, and 450nm for all samples S1, S2, S3, and S4 are observed. On increasing Sulphur Cu the intensity is reduced and the broadness of luminescence peaks decreases.

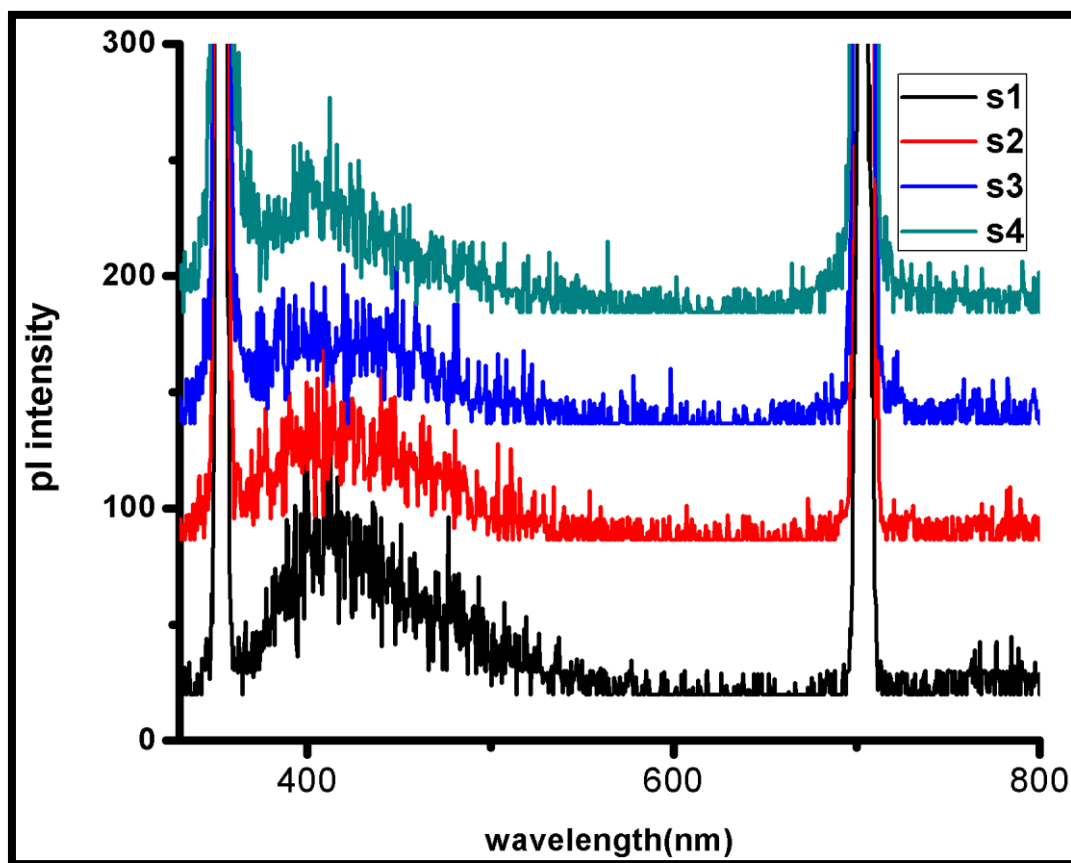


Fig. 5. PL spectra of CuS nanocomposites

### 3.5 Photocatalytic activity

As the samples are exposed to increasing light intensity and longer illumination times, a reduction in dye absorption becomes evident. This trend is depicted graphically in Figure 6, illustrating a decline in dye concentration with light irradiation. It is worth noting that the incorporation of Cu within the photocatalyst system plays a pivotal role in enhancing carrier separation and augmenting light absorption. Similar observations were reported [39-41].

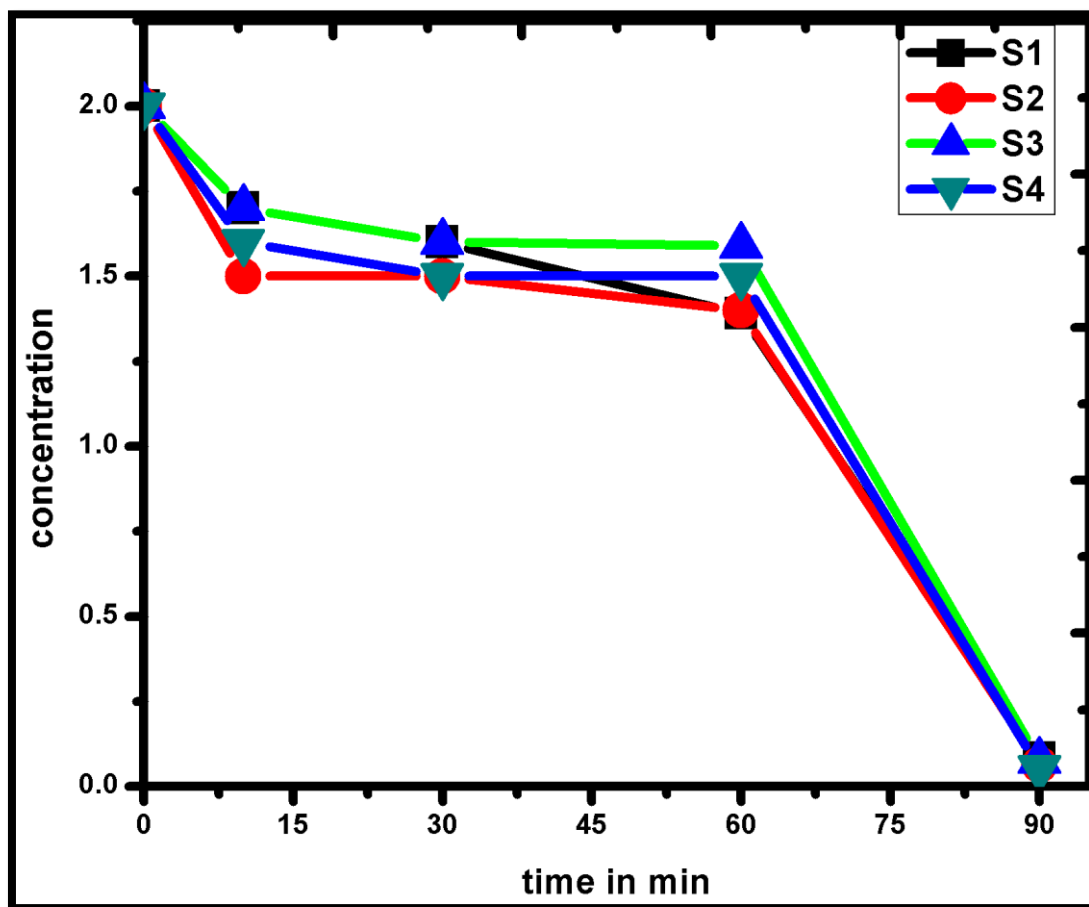


Fig. 6. Concentration vs. time graph of CuS nanocomposite for MR dye

### 3.5.1 Percentage degradation of dyes

The percentage of photocatalytic degradation was computed using equation (1). A graphical representation of the per cent degradation is presented in Fig. 7. As the sulphur (S) content in the Cu ratio decreases, the decomposition rate attains a value of 93.9%. Conversely, the decomposition rate exhibits an increase in tandem with elevated S content within the Cu. Remarkably, the fourth sample, harbouring a substantial proportion of S nanoparticles in Cu, achieves an impressive 96.3% dye removal from the water in a mere 190 minutes. For comprehensive information on the calculated rate constants and degradation rate values, kindly refer to Table 2.

Table 2. Rate constant and degradation value

Samples	S1	S2	S3	S4
Rate constant(K)	0.00393	0.004	0.00393	0.00403
Degradation %	93.9	95.7	95.3	96.3

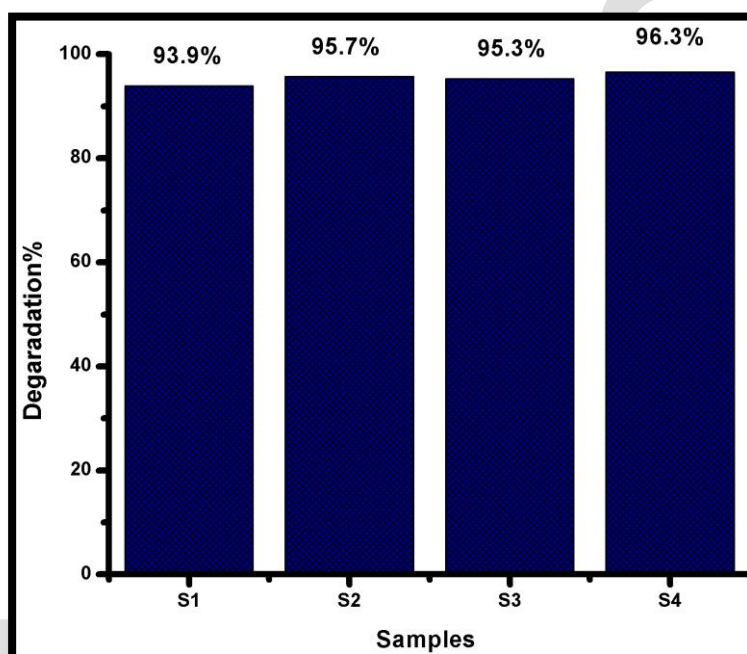


Fig. 7. Histogram of Percentage degradation in photocatalytic activity

### 3.5.2 Mechanism of the chemical equation

The photocatalytic activity was conducted using a 36-watt LED light setup for a duration of 190 minutes. In this assessment, the degradability of the catalyst was examined using methyl red dye. A depiction of the photocatalytic activity mechanism involving MR dye and CuS nanoparticles is presented in Figure 8. When the incident light encounters the catalyst, it initiates the generation of electrons and holes. The adsorption mechanism involves electrostatic repulsion between the dye and the CuS catalyst nanoparticles. Among the samples, S4 exhibited superior degradation performance.

Notably, since methyl red is an anionic dye, it interacts with the holes within the catalyst, leading to its decomposition [39-41]. Moreover, these holes react with hydroxyl ions, yielding additional  $\text{OH}^*$  free

radicals, which contribute to the degradation process. The concentration versus time graph assumes a linear profile, consistent with a first-order kinetic pseudo-reaction [41].

Under UV-Visible light photocatalytic activity due to absorption of photon electrons and holes in CuS moves to conduction and valance bands respectively. The electrons on the surface of conduction band of CuS reacts with oxygen molecules to generate superoxide ( $O_2^{\cdot-}$ ) anion radicals [42], and the separated holes in the valence bands of CuS effectively oxidize  $H_2O$  into hydroxyl radicals ( $OH^{\cdot}$ ) [43]. Consequently, the  $OH^{\cdot}$  and  $O_2^{\cdot-}$  radicals react with Methyl red dye and degrade them into nontoxic and inorganic products (e.g.,  $H_2O$  and  $CO_2$ ). The operating mechanism is illustrated in Figure 8

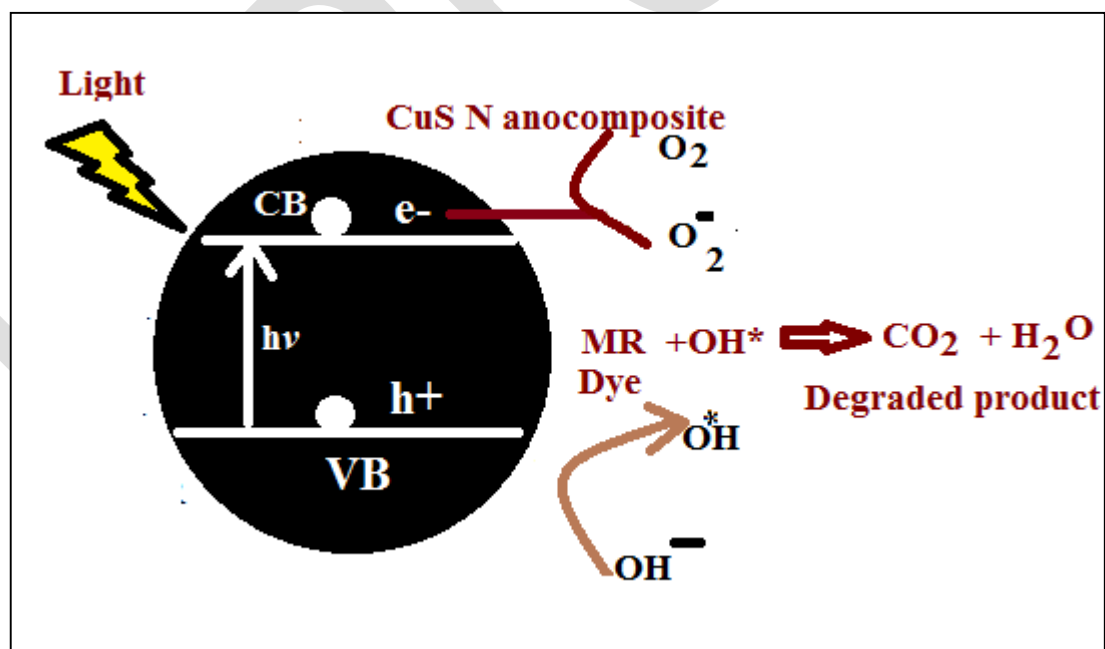
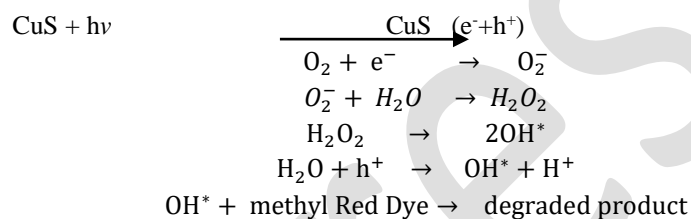


Fig. 8. Mechanism of photocatalytic activity of MR dye with CuS nanoparticles

#### 4. Conclusions

In this study, we successfully synthesised CuS nanoparticles (NPs) with nanometer-scale dimensions utilizing a wet chemical method. The XRD pattern unequivocally verified the hexagonal phase presence within the CuS particles. Notably, the investigation also unveiled a slightly sulfur-rich CuS NPs variant with an estimated bandgap energy of 3.8eV. Remarkably, this energy surpasses that of bulk CuS (1.85eV), signifying a significant miniaturisation effect. The synthesized CuS NPs exhibited outstanding photocatalytic activity in the degradation of methyl Red (MR), showcasing remarkable efficiency under visible light irradiation. Sample S4 shows the best photocatalytic activity. This performance can be attributed to the presence of surface-bound OH ions on the CuS nanostructures, which facilitate the adsorption and acceleration of the degradation process for MR molecules. The catalyst managed to degrade 96.3% of the methyl red dye within just 190 minutes using a 0.2g quantity, with higher sulphur ratio CuS nanostructures demonstrating the highest efficacy in achieving this remarkable degradation efficiency. Thus our result is better than reported by many research group on Photocatalytic activity of CuS nanoparticles on dyes like MB(Methylene blue),CR(Congo Red),RhB (Rhodamine B),[27-29] with percentage degradation ranging from 50 to 94.

## References:

1. Alivisatos, A. P., "Semiconductor Clusters, Nanocrystals and Quantum Dots." *Science* 1996, 271 (5251), 933–937.
2. Gahlaut, U. P. S., Kumar, V., Pandey, R. K., Goswami, Y. C. "Highly Luminescent Ultra Small Cu Doped ZnO Nanostructures Grown by Ultrasonicated Sol–Gel Route." *Optik* 2016, 127(10), 4292–4295.
3. Kshirsagar, U. A., Joshi, D. C., "Advancement in Fabrication of Sensors Using Nanotechnology: A Bibliographic Review and Future Research Scope." *Adv. Nano Res.* 2023, 14(5), 399–407.
4. Kumar, N., Purohit, L. P., Goswami, Y. C., "Spin Coating of ZnS Nanostructures on Filter Paper and Their Characterization." *Phys. E: Low-Dimens. Syst. Nanostruct.* 2016, 83, 333–338.
5. Zhao, L., Zhou, L., Sun, C., Gu, Y., Wen, W., Fang, X., "Rose-Like CuS Microflowers and Their Enhanced Visible-Light Photocatalytic Performance." *CrystEngComm* 2018, 20, 6529–6537.
6. Riyaz, S., Parveen, A., Azam, A., "Microstructural and Optical Properties of CuS Nanoparticles Prepared by Sol-Gel Route." *Perspect. Sci.* 2016, 8, 632–635.
7. Ding, T. Y., Wang, M. S., Guo, S. P., Guo, G. C., Huang, J. S., "CuS Nanoflowers Prepared by a Polyol Route and Their Photocatalytic Property." *Mater. Lett.* 2008, 62(30), 4529–4531.
8. Chen, Y. B., Chen, L., Wu, L. M., "Water-Induced Thermolytic Formation of Homogeneous Core-Shell CuS Microspheres and Their Shape Retention on Desulfurization." *Cryst. Growth Des.* 2008, 8 (8), 2736–2740.

9. Shamraiz, U., Hussain, R. A., Badshah, A., "Fabrication and Applications of Copper Sulfide (CuS) Nanostructures." *J. Solid State Chem.* 2016, 238, 25–40.
10. Han, Y., Wang, Y., Gao, W., Wang, Y., Jiao, L., Yuan, H., Liu, S., "Synthesis of Novel CuS with Hierarchical Structures and Its Application in Lithium-Ion Batteries." *Powder Technol.* 2011, 212 (1), 64–68.
11. Noor ul Ain, Nasir, J. A., Khan, Z., Butler, I. S., Rehman, Z., "Copper Sulfide Nanostructures: Synthesis and Biological Applications." *RSC Adv.* 2022, 12, 7550.
12. Basu, M., Sinha, A. K., Pradhan, M., Sarkar, S., Negishi, Y., Pal, T., "Synthesis and Characterization of a Bi-Oxide Nanoparticle ZnO/CuO by Thermal Decomposition of Oxalate Precursor Method." *Int. J. Nano Dimens.* 2010, 1 (1), 33–40.
13. Wang, L., "Synthetic Methods of CuS Nanoparticles and Their Applications for Imaging and Cancer Therapy." *RSC Adv.* 2016, 6, 82596–82615.
14. Ghane, M., Sadeghi, B., Jafari, A., Paknejad, A., "Synthesis and Characterization of a Bi-Oxide Nanoparticle ZnO/CuO by Thermal Decomposition of Oxalate Precursor Method." *Int. J. Nano Dimens.* 2010, 1 (1), 33–40.
15. Sadeghi, B., Ghammamy, S., Gholipour, Z., Ghorchibeigy, M., Amini Nia, A., "Gold/Hydroxypropyl Cellulose Hybrid Nanocomposite Constructed with More Complete Coverage of Gold Nano-Shell." *Micro Nano Lett.* 2011, 6, 209–213.
16. He, W., Jia, H., Li, X., Lei, Y., Li, J., Zhao, H., Mi, L., Zhang, L., Zheng, Z., "Understanding the Formation of CuS Concave Superstructures with Peroxidase-Like Activity." *Nanoscale* 2012, 4, 3501–3506.
17. Kaundal, J. B., Goswami, Y. C., Sharma, R., "Optically Important Transparent Syndiotactic Polystyrene/FeS Composites Grown by Low Sol-Gel Route." *Orient. J. Chem.* 2022, 38 (3), 766–770.
18. Cheng, Z., Wang, S., Wang, Q., Geng, B., "A Facile Solution Chemical Route to Self-Assembly of CuS Ball-Flowers and Their Application as an Efficient Photocatalyst." *CrystEngComm* 2010, 12, 144–149.
19. Murugan, S., Garg, S., Singh, I., Rajendran, R., Santhosh, C., Chevva, H., Vanchinathan, T., Marepally, B., Grace, A., "Solvothermal Preparation of ZnO/Graphene Nanocomposites and Its Photocatalytic Properties." *Nanoscience Nanotechnol. Lett.* 2013, 5, 349–354.
20. Roy, P., Srivastava, S. K., "Solvothermal Growth of Flowerlike Morphology from Nanorods of Copper Sulfides." *J. Nanoscience Nanotech.* 2008, 8 (3), 1523–1527.
21. Palanisamy, S., Velmurugan, S., Yang, T. C. K., "One-Pot Sonochemical Synthesis of CuS Nanoplates Decorated Partially Reduced Graphene Oxide for Biosensing of Dopamine Neurotransmitter." *Ultrason. Sonochem.* 2020, 64, 105043.
22. Kumar, N., Pathak, T. K., Purohit, L. P., Swart, H. C., Goswami, Y. C., "Self-Assembled Cu Doped CdS Nanostructures on Flexible Cellulose Acetate Substrates Using Low-Cost Sol-Gel Route." *Nano-Structures Nano-Objects* 2018, 16, 1–8.
23. Mezgebe, M. M., Ju, A., Wei, G., Macharia, D. K., Guang, S., Xu, H., "Structure-Based Optical Properties and Catalytic Activities of Hydrothermally Prepared CuS Nanostructures." *Nanotech* 2019, 30 (1), 105704.

24. Zhang, P., Gao, L., "Copper Sulfide Flakes and Nanodisks." *J. Mater. Chem.* 2003, *13* (8), 2007–2010.
25. Xu, H. L., Wang, W. Z., Zhu, W., "Sonochemical Synthesis of Crystalline CuS Nanoplates via an In Situ Template Route." *Mater. Lett.* 2006, *60* (17–18), 2203–2206.
26. Du, W., Qian, X., Xiaodong, M., Gong, Q., Cao, H., Yin, J., "Shape-Controlled Synthesis and Self-Assembly of Hexagonal Covellite (CuS) Nanoplatelets." *Chemistry* 2007, *13* (11), 3241–3247.
27. Ayodhya, D., Venkatesham, M., Kumari, A. S., Reddy, G. B., Ramakrishna, D., Veerabhadram, G., "Photocatalytic Degradation of Dye Pollutants under Solar, Visible, and UV Lights Using Green Synthesized CuS Nanoparticles." *J. Exp. Nanosci.* 2016, *11*, 418–432.
28. Wu, H., Li, Y., Li, Q., "Facile Synthesis of CuS Nanostructured Flowers and Their Visible Light Photocatalytic Properties." *Appl. Phys. A* 2017, *123*, 196.
29. Nancucheo, A., Segura, A., Hernandez, P., Hernandez-Montelongo, J., Pesenti, H., Arranz, A., Benito, N., Romero-Saez, M., Contreras, B., Díaz, V., et al. "Covellite Nanoparticles with High Photocatalytic Activity Bioproduced by Using H<sub>2</sub>S Generated from a Sulfidogenic Bioreactor." *J. Environ. Chem. Eng.* 2022, *10*, 107409.
30. Saranya, M., Grace, A. N., "Hydrothermal Synthesis of CuS Nanostructures with Different Morphology." *J. Nano Res.* 2012, *18–19*, 43–51.
31. Umair, S., Hussain, A., Badshah, A., "Fabrication and Applications of Copper Sulfide (CuS) Nanostructures." *J. Solid State Chem.* **2016**, *238*, 25–40..
32. Savarimuthu, I., Susairaj, M. J. A. M., "CuS Nanoparticles Trigger Sulphite for Fast Degradation of Organic Dyes under Dark Conditions." *ACS Omega* **2022**, *7* (5), 4140–4149.
33. Roy, P., Srivastava, S. K., "Nanostructured Copper Sulfides: Synthesis, Properties and Applications." *CrystEngComm* **2015**, *17*, 7801–7815..
34. Mote, V., Purushotham, Y., Dole, B., "Williamson-Hall Analysis in Estimation of Lattice Strain in Nanometer-Sized ZnO Particles." *J. Theor. Appl. Phys.* **2012**, *6*, 6.
35. Cullity, B. D., Stock, S. R., "Elements of X-Ray Diffraction". 3rd ed.; Prentice-Hall Inc.: Upper Saddle River, NJ, 2001; pp 167–171.
36. Riyaz, S., Parveen, A., Azam, A., "Microstructural and Optical Properties of CuS Nanoparticles Prepared by Sol-Gel Route." *Perspect. Sci.* 2016, *8*, 632–635.
37. Koutu, V., Rajawat, S., Shastri, L., Malik, M. M., "Apoptosis and Inhibition of Human Epithelial Cancer Cells by ZnO Nanoparticles Synthesized Using Plant Extract." *Adv. Nano Res.* 2019, *7* (4), 233–240.
38. Kumar, N., Purohit, L. P., Goswami, Y. C., "Spin Coating of Highly Luminescent Cu Doped CdS Nanorods and Their Optical Structural Characterizations." *Chal. Lett.* 2015, *12* (6), 333–338.
39. Kumar, N., Purohit, L. P., Goswami, Y. C., "Synthesis of Cu Doped ZnS Nanostructures on Flexible Substrate Using Low-Cost Chemical Method". *AIP Conf. Proc.* 2015, *1675* (1), 020030.
40. Nagaich, S., Goswami, Y. C., "Shor's Algorithm for Quantum Numbers Using MATLAB Simulator." *Proc. 5th Int. Conf. Adv. Comput. Commun. Technol.* 2015, *5*, 165–168.

41. Zhu, S., Wang, D., "Photocatalysis: Basic Principles, Diverse Forms of Implementations and Emerging Scientific Opportunities." *Adv. Energy Mater.* 2017, 7 (23), 1700841.
42. Lv, M., Yang, L., Wang, X., Cheng, X., Song, Y., Yin, Y., Liu, H., Han, Y., Cao, K., Ma, W., Qi, G., Li, S., "Visible-Light Photocatalytic Capability and the Mechanism Investigation of a Novel PANI/Sn<sub>3</sub>O<sub>4</sub> p–n Heterostructure." *RSC Adv.* 2019, 9, 40694–40707.
43. Ali, M. E., Alhathal, A. A., Azeez, F. A., Ghaly, M. Y., "Photoassisted Mineralization of Remazole Red F3B over NiO/TiO<sub>2</sub> and CdO/TiO<sub>2</sub> Nanoparticles under Simulated Sunlight." *Sep. Sci. Technol.* 2018, 53, 170–180.

In Press